JOURNAL OF GUIDANCE, CONTROL, AND DYNAMICS
Vol. 23, No. 4, July–August 2000

Design of Lifted Dual-Rate Digital Controllers for X-38 Vehicle

Leang-San Shieh* and Wei-Min Wang†
University of Houston, Houston, Texas 77204-4793
John Bain‡
NASA Johnson Space Center, Houston, Texas 77058
and
John W. Sunkel§
University of Colorado at Boulder, Boulder, Colorado 80309-0422

A new state-matching digital redesign method to find the lifted dual-rate pulse-amplitude-modulated (PAM) and pulse-width-modulated (PWM) digital controllers from a predesigned, state-feedback, continuous-time controller is presented. The proposed method provides close matching of the states of the continuous-time controlled analog system with those of the digitally redesigned system (including intersample behavior). The redesigned lifted dual-rate controller enables the digitally controlled X-38 vehicle to track the desired trajectory while remaining insensitive to modeling parameters, initial conditions, and exogenous disturbances for larger sample times than existing methods. The X-38 will require a PAM controller for commanding the electromechanical actuators that operate its aerodynamic surfaces for flight in the atmosphere. PWM control will be used to command the reaction control jets during orbital operations. The proposed method provides a new alternative for indirect digital design of state-feedback multivariable continuous-time systems.

I. Introduction

THE X-38 is a set of prototype flight test vehicles for the crew return vehicle (CRV)[1] that is being designed and tested for the International Space Station by NASA Johnson Space Center (JSC). The CRV will give space station personnel a way of returning to Earth in the event of an emergency such as 1) a catastrophic emergency aboard the station, 2) a medical emergency on the station and 3) the lack of ground support for a period of time. The test vehicles will be designed, built, and tested by JSC to study vehicle characteristics such as flight dynamics, vehicle/parafoil interactions, guidance, navigation, and control. The operational crew return vehicles will be built in late 2002.

The dynamic equations of the X-38 vehicle were recently developed by Bain and Sunkel.[2] In Ref. 2, an X-38 flight control system is designed in the continuous-time domain using a state-feedback linear quadratic regulator (LQR) for tracking the desired trajectory. The availability of high-performance, low-cost microprocessors and associated digital electronics has led to the development of digital controllers for the (continuous domain) X-38 flight vehicles. Hence, in the actual flight control of the X-38, it is required to develop digital controllers that can be implemented in a 68040 processor running at 25 Hz, that is, the sampling period $T = 0.04$ s (Ref. 2).

There exist three digital design approaches for state-feedback digital control systems. The first approach, called the direct digital design approach, is to discretize the analog plant and then determine a state-feedback digital controller for the discretized plant[3–10]; the second approach, called the digital redesign approach,[3,5,11–13] is to predesign a state-feedback analog controller for the analog plant and then carry out the digital redesign for the predesigned analog controller; and the third approach, called the direct sampled-data approach,[14] is to directly design a state-feedback digital controller for the analog plant, which is still under development.[15]

In general, there exist two types of digital controllers: the pulse-amplitude-modulated (PAM) controller[3–5,8,11–13] and the pulse-width-modulated (PWM) controller.[6,7,9,10,12] The PAM controller, which produces a series of piecewise-constant continuous pulses having a variable amplitude and variable or fixed width, is commonly utilized in digital control of all types. The PWM controller, which produces a series of discontinuous pulses with a fixed amplitude and variable width, has become popular in industry[16] for on–off control of dc power converter and stepper motors (widely used in robotics), satellite station keeping (with on–off reaction jets), etc. Because the direct digital design approach takes into account only the sampling instants of the continuous-time system, the resulting PAM and PWM controllers could produce degradation in the intersample behavior of the closed-loop sampled-data system.[17,18] Hence, we focus on the digital redesign approach for the development of the lifted PAM and PWM controllers in this paper.

II. New Lifted Dual-Rate State-Matching Digital Redesign Method

The lifting technique[8] transforms an m-input, P-output, N-periodic multirate discrete-time system into an equivalent mN-input, PN-output, single-rate linear time-invariant discrete-time system. As a result, the lifted single-rate discrete-time system is able to capture intersample behavior of the original system and allows standard discrete-time control techniques to be applied. The algebraic and analytical properties of the lifted system can be found in Ref. 15.

A. Continuous-Time Controller

Consider a controllable and observable continuous-time plant represented by

$$\dot{x}_c(t) = Ax_c(t) + Bu_c(t), \qquad x_c(0) = x_{c0}, \tag{1a}$$

$$y_c(t) = Cx_c(t) + Du_c(t) \tag{1b}$$

where $x_c(t) \in \Re^{n\times 1}$, $u_c(t) \in \Re^{m\times 1}$, and $y_c(t) \in \Re^{p\times 1}$. The optimal state-feedback control law that minimizes the performance index[19]

$$J = \int_0^\infty \left\{ [Cx_c(t) - r(t)]^T Q[Cx_c(t) - r(t)] + u_c^T(t) R u_c(t) \right\} \mathrm{d}t \tag{2}$$

where $Q \geq 0$ and $R > 0$ for the system in Eq. (1) having $D = 0$ is

$$u_c(t) = -K_c x_c(t) + E_c r(t) \tag{3}$$

Received 13 July 1998; revision received 20 September 1999; accepted for publication 24 October 1999.

*Professor, Department of Electrical and Computer Engineering. Associate Fellow AIAA.
†Graduate Student, Department of Electrical and Computer Engineering.
‡National Research Council Associate. Member AIAA.
§Adjunct Professor, Department of Aerospace Engineering. Associate Fellow AIAA.

In Eq. (3)

$$K_c = R^{-1}B^TP \tag{4a}$$

$$E_c = -R^{-1}B^T(A - BK_c)^{-T}C^TQ \tag{4b}$$

where $r(t)$ is a reference input and P is the solution of

$$A^TP + PA - PBR^{-1}B^TP + C^TQC = 0 \tag{5}$$

It is desirable to carry out digital redesign of the continuous-time state-feedback controller in Eq. (3) using a newly developed lifted dual-rate state-matching digital redesign method.

B. PAM Controller Redesign Overview

The existing lifted methodology[8,13] for digital redesign of a continuous-time system is reviewed in this section. Let $u_c(t)$ in Eq. (1a) for $0 \le t < T_s$ be represented using an orthonormal series[20] [$\Phi_{k_f}(t)\Phi_{j_f}(t) = 0$ for $k_f \neq j_f$, $\Phi_{k_f}(t)\Phi_{j_f}(t) = \Phi_{k_f}(t)$ for $k_f = j_f$] as

$$u_c(t) \cong \sum_{k_f=1}^{N} W_{k_f}\Phi_{k_f}(t) \tag{6a}$$

where

$$\Phi_{k_f}(t) = \begin{cases} 1 & \text{for} \quad (k_f - 1)T_f \le t < k_fT_f \\ 0 & \text{otherwise} \end{cases} \tag{6b}$$

with $T_f = T_s/N$. T_f is a fast sampling period, N is the sampling ratio during a slow sampling period T_s, and

$$W_{k_f} = \frac{1}{T_f}\int_{k_fT_f}^{k_fT_f + T_f} u_c(t)\,dt \tag{6c}$$

For $u_c(t)$ slowly varying over the time interval k_fT_f–$k_fT_f + T_f$, it can be approximated using a multisegment rectangular rule as

$$u_c(t) \cong \sum_{k_f=1}^{N} \bar{W}_{k_f}\Phi_{k_f}(t) \triangleq \sum_{k_f=1}^{N} \bar{u}_{dk_f}(k_fT_f) \tag{7a}$$

where $\bar{W}_{k_f}$ can be approximately evaluated from Eq. (6c) as

$$W_{k_f} = \frac{1}{T_f}\int_{k_fT_f}^{k_fT_f + T_f} u_c(t)\,dt \cong u_c(t)|_{t=k_fT_f} \triangleq \bar{W}_{k_f} \tag{7b}$$

$$\bar{u}_{dk_f}(t) = u_c(k_fT_f)\Phi_{k_f}(t) \triangleq \bar{u}_{dk_f}(k_fT_f) \quad \text{for} \quad k_fT_f \le t < k_fT_f + T_f \tag{7c}$$

The corresponding sampled-data system in Eq. (1a) with a set of lifted fast-rate sampled input in Eq. (7a) becomes

$$\dot{x}_d(t) = Ax_d(t) + B\sum_{k_f=1}^{N} \bar{u}_{dk_f}(k_fT_f) \tag{8}$$

and the associated fast-sampled discrete-time system in Eq. (8) with $N = 1$ and $\bar{u}_{dk_f}(k_fT_f) \triangleq u_d(k_fT_f)$ becomes

$$x_d(k_fT_f + T_f) = G_Nx_d(k_fT_f) + H_Nu_d(k_fT_f) \tag{9}$$

where $G_N = e^{AT_f}$ and $H_N = [G_N - I_n]A^{-1}B$.

Note 1: When $A \in \Re^{n\times n}$ is a nonzero singular matrix, then $(e^{AT} - I_n)A^{-1}$, where T is a sampling period, can be represented as

$$\sum_{i=1}^{\infty} \frac{(AT)^{i-1}T}{i!}$$

The associated discrete-time model in Eq. (8) for a slow-sampled system with a lifted fast-sampled input for $k_sT_s \le t < k_sT_s + T_s$ and $k_sT_s = k_fT_f$ can be written as

$$x_d(k_sT_s + T_s) = G_N^Nx_d(k_sT_s) + \bar{H}_N^{(N)}\bar{u}_d^{(N)}(k_sT_s) \tag{10}$$

where the lifted system matrix G_N^N is

$$G_N^N = (G_N)^N = e^{AT_s}$$

the lifted input matrix $\bar{H}_N^{(N)}$ is defined as

$$\bar{H}_N^{(N)} \triangleq [\bar{H}_1, \bar{H}_2, \ldots, \bar{H}_{N-1}, \bar{H}_N] = \left[G_N^{N-1}H_N, G_N^{N-2}H_N, \ldots, G_NH_N, H_N\right] \in \Re^{n\times mN}$$

the lifted input vector $\bar{\boldsymbol{u}}_d^{(N)}(k_sT_s)$ is defined as

$$\bar{\boldsymbol{u}}_d^{(N)}(k_sT_s) \triangleq \left[\bar{u}_{d1}^T(k_sT_s), \bar{u}_{d2}^T(k_sT_s), \ldots, \bar{u}_{dN}^T(k_sT_s)\right]^T = \left[u_c^T(k_sT_s), u_c^T(k_sT_s + T_f), \ldots, u_c^T(k_sT_s + (N-1)T_f)\right]^T \in \Re^{mN\times 1}$$

$\bar{H}_i \triangleq G_N^{N-i}H_N$ with $H_N = (G_N - I_n)A^{-1}B$ and $\bar{u}_{di}(k_sT_s) \triangleq u_c(t)$ at $t = k_sT_s + (i-1)T_f$ for $i = 1, 2, \ldots, N$.

The discrete-time system in Eq. (10) can be considered as a multi-input/multi-output (MIMO) digital model. Hence, any MIMO discrete-time design method can be utilized to design a lifted state-feedback control law for the system in Eq. (10) as

$$\bar{\boldsymbol{u}}_d^{(N)}(k_sT_s) = -\bar{K}_d^{(N)}x_d(k_sT_s) + \bar{E}_d^{(N)}r(k_sT_s) \tag{11a}$$

where the lifted control gains $\bar{K}_d^{(N)}$ and $\bar{E}_d^{(N)}$ are defined as

$$\bar{K}_d^{(N)} \triangleq \left[K_{d_1}^T, K_{d_2}^T, \ldots, K_{d_N}^T\right]^T \in \Re^{mN\times n} \tag{11b}$$

$$\bar{E}_d^{(N)} \triangleq \left[E_{d_1}^T, E_{d_2}^T, \ldots, E_{d_N}^T\right]^T \in \Re^{mN\times m} \tag{11c}$$

where $r(t) = r(k_sT_s)$ for $k_sT_s \le t < k_sT_s + T_s$ is a reference input. The digitally designed system is

$$x_d(k_sT_s + T_s) = \left(G_N^N - \bar{H}_N^{(N)}\bar{K}_d^{(N)}\right)x_d(k_sT_s) + \bar{H}_N^{(N)}\bar{E}_d^{(N)}r(k_sT_s) \tag{12}$$

The aforementioned method for digital design of a continuous-time system can be called a lifted dual-rate digital design method.[8,17]

An alternative lifted dual-rate digital redesign method, called a generalized digital redesign method[13] that matches the states at multiple sampling periods (k_sT_s for $k_s = 1, 2, \ldots$), can be described as follows. Let a continuous-time control law for the continuous-time system (1a) be represented as

$$u_c(t) = -K_cx_c(t) + E_cr(t) \tag{13}$$

where K_c and E_c are available analog gains. Then, the designed continuous-time system is

$$\dot{x}_c(t) = A_cx_c(t) + BE_cr(t) \tag{14}$$

where $A_c = A - BK_c$, and the corresponding discrete-time model for $r(t) = r(k_sT_s)$ with $k_sT_s \le t < k_sT_s + T_s$ is

$$x_c(k_sT_s + T_s) = G_cx_c(k_sT_s) + H_cE_cr(k_sT_s) \tag{15}$$

where $G_c = e^{A_cT_s}$, $A_c = A - BK_c$, and $H_c = (G_c - I_n)A_c^{-1}B$.

For exactly matching the discrete-time state $x_c(k_sT_s)$ in Eq. (15) with the discrete-time state $x_d(k_sT_s)$ in Eq. (12) at multiple sampling

periods without considering the intersampling behavior, the lifted digital gains, $\bar{K}_d^{(N)}$ and $\bar{E}_d^{(N)}$ in Eq. (12) can be solved from the following matrix equations:

$$G_N^N - \bar{H}_N^{(N)} \bar{K}_d^{(N)} = G_c \tag{16a}$$

$$\bar{H}_N^{(N)} \bar{E}_d^{(N)} = H_c E_c \tag{16b}$$

The desired lifted digital gains in Eq. (11) are

$$\bar{K}_d^{(N)} = \left(\bar{H}_N^{(N)}\right)^+ \left(G_N^N - G_c\right) \tag{17a}$$

$$\bar{E}_d^{(N)} = \left(\bar{H}_N^{(N)}\right)^+ H_c E_c \tag{17b}$$

where $(\bar{H}_N^{(N)})^+ = (\bar{H}_N^{(N)})^T [\bar{H}_N^{(N)} (\bar{H}_N^{(N)})^T]^{-1}$ for $\text{rank}(\bar{H}_N^{(N)}) = n$ and $mN \geq n$.

It is observed that both the lifted dual-rate digital design method[8] and the generalized digital redesign method[13] utilize the conventional rectangular-rule approximation method and are able to capture the system's intersample behavior for a sufficiently large sampling ratio N. In other words, if the slow sampling period T_s is not sufficiently small and the sampling ratio $N(=T_s/T_f)$ is not sufficiently large, then the performance specifications based on the obtained discrete-time model could produce a degradation in the intersample behavior of the closed-loop sampled-data system even though a lifted fast-rate control law is utilized.[17,18] To improve the performance of the intersample behavior, we propose a new lifted dual-rate state-matching digital redesign method as follows.

C. Lifted Dual-Rate PAM Controller Redesign

Consider the continuous-time controlled closed-loop system in Eq. (14). The corresponding fast-sampled discrete-time system for $r(t) = r(k_f T_f)$ with $k_f T_f \leq t < k_f T_f + T_f$ is

$$x_c(k_f T_f + T_f) = G_{cN} x_c(k_f T_f) + H_{cN} E_c r(k_f T_f) \tag{18}$$

where $G_{cN} = e^{A_c T_f}$, $A_c = A - BK_c$, and $H_{cN} = [G_{cN} - I_n] A_c^{-1} B$. The associated slow-sampled discrete-time system for $r(t) = r(k_s T_s)$ with $k_s T_s \leq t < k_s T_s + T_s$ and $T_s = NT_f$ is

$$x_c(k_s T_s + T_s) = G_c x_c(k_s T_s) + H_c E_c r(k_s T_s) \tag{19}$$

where $G_c = (G_{cN})^N$ and $H_c = [G_c - I_n] A_c^{-1} B$.

It is desirable to find the lifted dual-rate digitally redesigned control law,

$$\bar{\boldsymbol{u}}_d^{(N)}(k_s T_s) \triangleq \left[\bar{u}_{d1}^T(k_s T_s), \bar{u}_{d2}^T(k_s T_s), \ldots, \bar{u}_{dN}^T(k_s T_s)\right]^T$$

$$= \left\{u_{d1}^T(k_s T_s), u_{d2}^T(k_s T_s + T_f), \ldots, u_{dN}^T[k_s T_s + (N-1)T_f]\right\}^T$$

$$= -\bar{K}_d^{(N)} x_d(k_s T_s) + \bar{E}_d^{(N)} r(k_s T_s) \tag{20}$$

from the analog control law in Eq. (13) such that the closed-loop state $x_c(t)$ in Eq. (14) closely matches that of the digitally redesigned sampled-data state $x_d(t)$ at $t = k_f T_f + iT_f$ for $i = 0, 1, 2, \ldots$ and any k_f. In Eq. (20), $x_d(t)$ is the state of the following lifted fast-rate sampled-data system (8)

$$\dot{x}_d(t) = A x_d(t) + B \sum_{k_f=1}^{N} \bar{u}_{dk_f}(k_f T_f) \tag{21}$$

The desired control of Eq. (20) is presented in the following theorem.

Theorem 1: Consider the open-loop continuous system in Eq. (1a) with a set of lifted fast-rate piecewise-constant inputs $u_{di}(t) = u_{di}[k_s T_s + (i-1)k_f] \triangleq \bar{u}_{di}(k_s T_s)$ for $k_s T_s + (i-1)T_f \leq t < k_s T_s + iT_f$ and $i = 1, 2, \ldots, N$ as

$$\dot{x}_d(t) = A x_d(t) + B \sum_{i=1}^{N} u_{di}[k_s T_s + (i-1)T_f] \tag{22}$$

The corresponding discrete-time model for a slow-sampled system with a lifted fast-sampled input for $k_s T_s \leq t < k_s T_s + T_s$ is shown in Eq. (10) as

$$x_d(k_s T_s + T_s) = G_N^N x_d(k_s T_s) + \bar{H}_N^{(N)} \bar{\boldsymbol{u}}_d^{(N)}(k_s T_s) \tag{23a}$$

$$= G_N^N x_d(k_s T_s) + \sum_{i=1}^{N} \bar{H}_i u_{di}[k_s T_s + (i-1)T_f] \tag{23b}$$

The lifted dual-rate state-matching PAM digital control law $\bar{\boldsymbol{u}}_d^{(N)}(k_s T_s)$ in Eq. (23a), which enables us to closely match the closed-loop state $x_d(t)$ in Eq. (22) with the closed-loop state $x_c(t)$ in Eq. (14) at $t = k_s T_s + iT_f$ with $i = 0, 1, \ldots, N-1$ for $r(t) = r(k_s T_s)$ with $k_s T_s \leq t < k_s T_s + T_s$, is

$$\bar{\boldsymbol{u}}_d^{(N)}(k_s T_s) \triangleq \left[\bar{u}_{d1}^T(k_s T_s), \bar{u}_{d2}^T(k_s T_s), \ldots, \bar{u}_{dN}^T(k_s T_s)\right]^T$$

$$= \left\{u_{d1}^T(k_s T_s), u_{d2}^T(k_s T_s + T_f), \ldots, u_{dN}^T[k_s T_s + (N-1)T_f]\right\}^T$$

$$= -\bar{K}_d^{(N)} x_d(k_s T_s) + \bar{E}_d^{(N)} r(k_s T_s) \tag{24a}$$

where

$$\bar{K}_d^{(N)} \triangleq \left[\bar{K}_{d1}^T, \bar{K}_{d2}^T, \ldots, \bar{K}_{dN}^T\right]^T$$

$$= \left[K_{dk}^T, \left(K_{dk} \hat{G}_{cN}\right)^T, \ldots, \left(K_{dk} \hat{G}_{cN}^{N-1}\right)^T\right]^T \tag{24b}$$

$$\bar{E}_d^{(N)} \triangleq \left[\bar{E}_{d1}^T, \bar{E}_{d2}^T, \ldots, \bar{E}_{dN}^T\right]^T = \left[E_{dk}^T, (E_{dk} - K_{dk} \hat{H}_{cN})^T, \ldots,\right.$$

$$\left.\left(E_{dk} - \sum_{j=1}^{N-1} K_{dk} \hat{G}_{cN}^{N-1-j} \hat{H}_{cN}\right)^T\right]^T \tag{24c}$$

$$K_{dk} = K_c (A_c T_f)^{-1} (G_{cN} - I_n) \tag{24d}$$

$$E_{dk} = \left[I_m + (K_c - K_{dk}) A_c^{-1} B\right] E_c \tag{24e}$$

$$u_{di}[k_s T_s + (i-1)T_f] = -\bar{K}_{di} x_d(k_s T_s) + \bar{E}_{di} r(k_s T_s)$$

$$\text{for} \quad i = 1, 2, \ldots, N \tag{24f}$$

$G_N = e^{AT_f}$, $H_N = [G_N - I_n] A^{-1} B$, $A_c = A - BK_c$, $\hat{G}_{cN} = G_N - H_N K_{dk}$, $\hat{H}_{cN} = H_N E_{dk}$, $G_{cN} = e^{A_c T_f}$, $H_{cN} = [G_{cN} - I_n] A_c^{-1} B$, and K_c and E_c are the predesigned analog gains in Eq. (13).

Note 2: When $N = 1$ and $T_f = T_s$, the single-rate state-matching PAM digital control law in Eq. (24) becomes

$$u_d(k_s T_s) = -K_d x_d(k_s T_s) + E_d r(k_s T_s) \tag{25a}$$

where

$$K_d = K_c (A_c T_s)^{-1} (G_c - I_n) \tag{25b}$$

$$E_d = \left[I_m + (K_c - K_d) A_c^{-1} B\right] E_c \tag{25c}$$

$G_c = e^{A_c T_s}$ and $A_c = A - BK_c$.

Proof: Consider the fast sampling of the continuous system in Eq. (1a) with a piecewise-constant input $u_{dk}(k_f T_f)$ as

$$\dot{x}_d(t) = A x_d(t) + B u_{dk}(k_f T_f) \quad \text{for} \quad k_f T_f \leq t < k_f T_f + T_f \tag{26a}$$

The associated discrete-time model is

$$x_d(k_f T_f + T_f) = G_N x_d(k_f T_f) + H_N u_{dk}(k_f T_f) \tag{26b}$$

Let the desired digitally redesigned control law be

$$u_{dk}(k_f T_f) = -K_{dk} x_d(k_f T_f) + E_{dk} r(k_f T_f) \tag{26c}$$

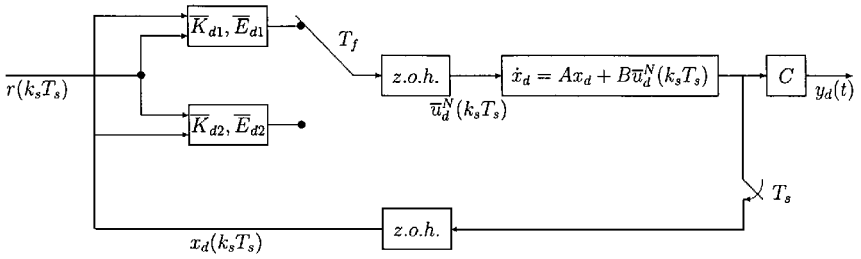

Fig. 1 Structure of the digitally redesigned sampled-data system ($N = 2$).

The corresponding closed-loop sampled-data system in Eq. (26a) using Eq. (26c) is

$$\dot{x}_d(t) = Ax_d(t) - BK_{dk}x_d(k_fT_f) + BE_{dk}r(k_fT_f) \tag{27a}$$

and its discrete-time model becomes

$$x_d(k_fT_f + T_f) = \hat{G}_{cN}x_d(k_fT_f) + \hat{H}_{cN}r(k_fT_f) \tag{27b}$$

For the same piecewise-constant reference input $r(t) = r(k_fT_f)$, it is desirable to find the digital gains K_{dk} and E_{dk} in Eq. (26c) so that the closed-loop state $x_d(t)$ in Eq. (27a) closely matches the closed-loop state $x_c(t)$ in Eq. (14) at $t = k_fT_f + iT_f$ for $i = 0$ and 1. The continuously varying control law $u_c(t)$ in Eq. (13) with a piecewise-constant reference input $r(t) = r(k_fT_f)$ can be approximately represented as

$$u_c(t) \cong W_{k_f}\Phi_{k_f}(t) \qquad \text{for} \qquad k_fT_f \le t < k_fT_f + T_f \tag{28a}$$

where

$$W_{k_f} = \frac{1}{T_f}\int_{k_fT_f}^{k_fT_f + T_f} u_c(t)\,\mathrm{d}t$$

$$= -\frac{K_c}{T_f}\int_{k_fT_f}^{k_fT_f + T_f} x_c(t)\,\mathrm{d}t + E_cr(k_fT_f) \tag{28b}$$

The state $x_c(t)$ in Eq. (28b) is the closed-loop state in Eq. (14), and the associated integral in Eq. (28b) can be exactly evaluated by integrating both sides of Eq. (14) as

$$x_c(k_fT_f + T_f) - x_c(k_fT_f)$$

$$= A_c\int_{k_fT_f}^{k_fT_f + T_f} x_c(t)\,\mathrm{d}t + T_fBE_cr(k_fT_f) \tag{29}$$

hence,

$$\int_{k_fT_f}^{k_fT_f + T_f} x_c(t)\,\mathrm{d}t = A_c^{-1}[x_c(k_fT_f + T_f) - x_c(k_fT_f)$$

$$- T_fBE_cr(k_fT_f)] \tag{30}$$

Substituting Eq. (18) into Eq. (30) and its result into Eq. (28b) yield a piecewise-constant input $u_c(t)$ in Eq. (28a). Substituting the obtained $u_c(t)$ into Eq. (1a) gives a sampled-data system. Then, discretizing the obtained sampled-data system yields the discrete-time closed-loop system as

$$x_c(k_fT_f + T_f)$$

$$= G_Nx_c(k_fT_f) - H_NK_c(A_cT_f)^{-1}(G_{cN} - I_n)x_c(k_fT_f)$$

$$+ H_N\left[I_m + K_cA_c^{-1}B - K_c(A_cT_f)^{-1}H_{cN}\right]E_cr(k_fT_f) \tag{31}$$

Letting $x_c(k_fT_f + T_f)$ and $x_c(k_fT_f)$ in Eq. (31) be equal to $x_d(k_fT_f + T_f)$ and $x_d(k_fT_f)$ in Eq. (27b), respectively, we have

$$G_N - H_NK_{dk} = G_N - H_NK_c(A_cT_f)^{-1}(G_{cN} - I_n) \tag{32}$$

and

$$H_NE_{dk} = H_N\left[I_m + (K_c - K_{dk})A_c^{-1}B\right]E_c \tag{33}$$

Solving Eqs. (32) and (33) gives the desired digitally redesigned gains K_{dk} and E_{dk} in Eqs. (24d) and (24e), respectively.

The desired lifted dual-rate digital control law $\bar{\boldsymbol{u}}_d^{(N)}(k_sT_s)$ in Eq. (24a) with a discrete-time state $x_d(k_sT_s)$ and $r(t) = r(k_sT_s)$ for $k_sT_s \le t < k_sT_s + T_s$ can be evaluated using the digital control law $u_d(k_fT_f)$ in Eq. (26c) as follows. Because $r(t) = r(k_sT_s)$ for $k_sT_s \le t < k_sT_s + T_s$, the digitally redesigned fast-sampled closed-loop system shown in Eq. (27b) can be utilized to evaluate the closed-loop state $x_d(t)$ in Eq. (27a) at $t = k_fT_f + (i-1)T_f$ and $k_fT_f = k_sT_s$ as

$$x_d[k_sT_s + (i-1)T_f] = \hat{G}_{cN}^{i-1}x_d(k_sT_s) + \sum_{j=1}^{i-1}\hat{G}_{cN}^{i-1-j}\hat{H}_{cN}r(k_sT_s) \tag{34}$$

Based on the definition of the lifted input in Eq. (24a), Eq. (26c) can be written as

$$u_{di}[k_sT_s + (i-1)T_f] = -K_{dk}x_d[k_sT_s + (i-1)T_f] + E_{dk}r(k_sT_s) \tag{35}$$

Substituting Eq. (34) into Eq. (35) and its result for $i = 1, 2, \ldots, N$ into Eq. (24a) yield the desired lifted digital control gains $\bar{K}_d^{(N)}$ and $\bar{E}_d^{(N)}$ in Eqs. (24b) and (24c), respectively. The structure of the PAM controlled dual-rate sampled-data system is shown in Fig. 1.

Remark 1: The conventional lifted dual-rate method utilizes a multisegment rectangular rule to approximately evaluate the coefficients $\bar{W}_{k_f}$ of the orthonormal series in Eq. (7b) for approximate representation of the continuous-time input $u_c(t)$ in Eq. (7a). Hence, the sampled-data system in Eq. (8) is a crude approximation of the original system in Eq. (1) if the $u_c(t)$ in Eq. (7a) or the control state $x_c(t)$ in Eq. (3) varies considerably during the sampling period. On the other hand, the proposed lifted dual-rate method employs an integration method in Eq. (29) to exactly evaluate the coefficients W_{k_f} of the orthonormal series in Eq. (28b) for close representation of the $u_c(t)$ in Eq. (28a). It is obvious that the proposed lifted dual-rate sampled-data model in Eq. (22) is superior to the conventional one in Eq. (8).

Moreover, in the conventional lifting technique, the lifted digital control law was constructed by directly utilizing the analog gains K_c and E_c in Eq. (13) as digital gains in conjunction with the discretized approximate state $x_d(k_fT_f)$ in Eq. (8). The proposed lifted digital control law is obtained using the state-matching digitally redesigned gains K_{dk} and E_{dk} in Eq. (24) together with the discretized approximate state $x_d(k_fT_f)$ in Eq. (22). When the sampling period T_f is sufficiently small, the digitally redesigned gains K_{dk} and E_{dk} can be reduced to the analog gains K_c and E_c by substituting $G_{cn} = e^{A_cT_f} \cong I_n + A_cT_f$ into the gains K_{dk} and E_{dk} in Eqs. (24d) and (24e). This implies that the conventional lifted digital control law is a specific class of the proposed one when the sampling period T_f is sufficiently small. In general, for a relatively longer sampling period, the proposed lifted dual-rate digital controllers would provide better results (including intersample behavior) than the conventional ones.

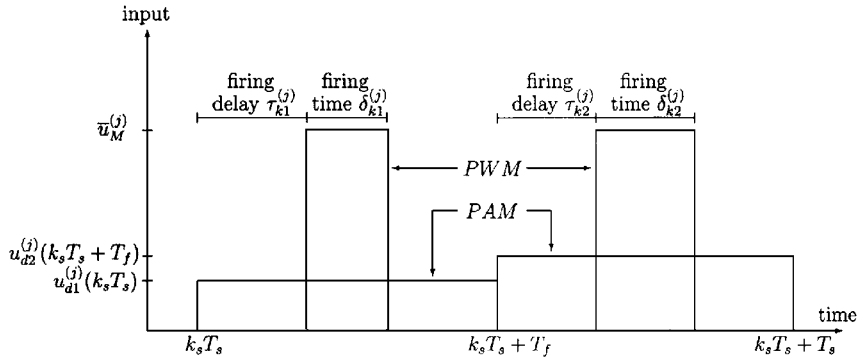

Fig. 2 Graphical illustration of PAM and PWM inputs ($N = 2$).

D. Ideal State Reconstruction

If the state $x_d(k_sT_s)$ in Eq. (24) is not available for measurement, the ideal state $x_d(k_sT_s)$ can be constructed[21,22] using the shifted and lifted fast-sampled input $u_c(t)$ [denoted by $\bar{u}_d^{(N)}(k_sT_s - T_s)$] and output $y_c(t)$ [denoted by $\bar{y}_d^{(N)}(k_sT_s - T_s)$] in Eq. (1) as

$$x_d(k_sT_s) = Q^+\left[\bar{y}_d^{(N)}(k_sT_s - T_s) + L\bar{u}_d^{(N)}(k_sT_s - T_s)\right] \tag{36}$$

In Eq. (36), $Q^+ = (Q^TQ)^{-1}Q^T$, $\text{rank}(Q) = n$, $mN \geq n$,

$$Q = \left\{\left[C\left(G_N^N\right)^{-1}\right]^T, \left[C\left(G_N^{N-1}\right)^{-1}\right]^T, \ldots, \left[C(G_N)^{-1}\right]^T\right\}^T$$

$$L = Q\bar{H}_N^{(N)} - \bar{L}$$

$$\bar{H}_N^{(N)} = \left[G_N^{N-1}H_N, G_N^{N-2}H_N, \ldots, G_NH_N, H_N\right]$$

$$\bar{L} = \begin{bmatrix} D & 0 & \cdots & 0 & 0 \\ CH_N & D & \cdots & 0 & 0 \\ CG_NH_N & CH_N & \cdots & 0 & 0 \\ CG_N^2H_N & CG_NH_N & \cdots & 0 & 0 \\ \cdots & & & & \\ CG_N^{N-1}H_N & CG_N^{N-2}H_N & \cdots & CH_N & D \end{bmatrix}$$

$$\bar{y}_d^{(N)}(k_sT_s - T_s) =$$

$$\left[y_d^T(k_sT_s - T_s), y_d^T(k_sT_s - T_s + T_f), \ldots, y_d^T(k_sT_s - T_f)\right]^T$$

$$\bar{u}_d^{(N)}(k_sT_s - T_s) =$$

$$\left[u_d^T(k_sT_s - T_s), u_d^T(k_sT_s - T_s + T_f), \ldots, u_d^T(k_sT_s - T_f)\right]^T$$

To accommodate the computational time delay[23] resulting from the use of the computed current state $x_d(k_sT_s)$ in Eq. (36), we compute the current control law in Eq. (24a), using the predicted state obtained from Eq. (23) instead of the current state $x(k_sT_s)$ as

$$\bar{u}_d^{(N)}(k_sT_s) = -\bar{K}_d^{(N)}\left[G_N^Nx_d(k_sT_s - T_s) + \bar{H}_N^{(N)}\bar{u}_d^{(N)}(k_sT_s - T_s)\right] + \bar{E}_d^{(N)}r(k_sT_s) \tag{37}$$

E. Lifted Dual-Rate PWM Controller Redesign

During on-orbit operation, the X-38 vehicle attitude is controlled with reaction jets.[2] These reaction jets require PWM as they fire with a fixed thrust for a desired length of time. The newly developed state-matching PAM digital controller in Theorem 1 can be employed to find a state-matching PWM digital control law as follows.

Lemma 1: Consider a controllable and observable system in Eq. (1) with a lifted dual-rate state-matching PWM digital control law as

$$\dot{x}_w(t) = Ax_w(t) + \sum_{i=1}^{N}\sum_{j=1}^{m} B^{(j)}u_{wi}^{(j)}(\lambda) \tag{38a}$$

$$y_w(t) = Cx_w(t) + \sum_{i=1}^{N}\sum_{j=1}^{P} D^{(j)}u_{wi}^{(j)}(\lambda) \tag{38b}$$

where $B^{(j)}$ and $D^{(j)}$ are the jth column of B and D, respectively, $u_{wi}^{(j)}(\lambda)$ is the jth component of the ith lifted PWM input vector. The lifted state-matching PWM digital control law $u_{wi}^{(j)}(\lambda)$, which enables us to closely match the PWM controlled state $x_w(t)$ in Eq. (38a) with the PAM controlled state $x_d(t)$ in Eq. (22) consists of the lifted PWM mode, shown in Fig. 2, as

$$u_{wi}^{(j)}(\lambda) = \begin{cases} 0, & k_sT_s + (i-1)T_f \leq \lambda < k_sT_s + (i-1)T_f + \tau_{ksi}^{(j)} \\ \bar{u}_M^{(j)}, & k_sT_s + (i-1)T_f + \tau_{ksi}^{(j)} \leq \lambda < k_sT_s \\ & \quad + (i-1)T_f + \tau_{ksi}^{(j)} + \delta_{ksi}^{(j)} \\ 0, & k_sT_s + (i-1)T_f + \tau_{ksi}^{(j)} + \delta_{ksi}^{(j)} \leq \lambda < k_sT_s + iT_f \end{cases} \tag{38c}$$

for $i = 1, 2, \ldots, N$ and $j = 1, 2, \ldots, m$. Here, $\bar{u}_M^{(j)}$, $\tau_{ksi}^{(j)}$, and $\delta_{ksi}^{(j)}$ are the jth input's fixed amplitude, firing delay, and firing duration in the ith lifted PWM input vector at the k_sth sampling, respectively. The firing duration and firing delay in the lifted PWM mode are

$$\delta_{ksi}^{(j)} = T_f\frac{\bar{u}_{di}^{(j)}(k_sT_s)}{\bar{u}_M^{(j)}}, \qquad \tau_{ksi}^{(j)} = \frac{1}{2}\left(T_f - \delta_{ksi}^{(j)}\right) \tag{38d}$$

where $\bar{u}_{di}^{(j)}(k_sT_s)$ is the jth component of the ith lifted PAM input vector in $\bar{u}_d^{(N)}(k_sT_s)$ as shown in Eq. (24a).

Note 3: When $N = 1$ and $T_f = T_s$, the single-rate state-matching PWM digital control law can be determined from Eqs. (38c) and (38d) letting $N = 1$ and $T_f = T_s$ in Eqs. (38c) and (38d) and utilizing the PAM digital control law in Eq. (25).

Proof: We write the lifted sampled-data system in Eq. (22) in an alternative form as

$$\dot{x}_d(t) = Ax_d(t) + \sum_{i=1}^{N}\sum_{j=1}^{m} B^{(j)}\bar{u}_{di}^{(j)}(k_sT_s) \tag{39}$$

Also, we write an alternative discrete-time model in Eq. (23) for the system in Eq. (39) as

$$x_d(k_sT_s + T_s) = G_N^Nx_d(k_sT_s) + \sum_{i=1}^{N}\sum_{j=1}^{m}\bar{H}_i^{(j)}\bar{u}_{di}^{(j)}(k_sT_s) \tag{40}$$

where $\bar{H}_i^{(j)} = G_N^{N-i}(G_N - I_n)A^{-1}B^{(j)}$.

The discrete-time model of the sampled-data system in Eqs. (38a) and (38c) can be written as

$$x_w(k_sT_s + T_s) = G_N^N x_w(k_sT_s) + \sum_{i=1}^{N}\sum_{j=1}^{m}\int_{k_sT_s+(i-1)T_f+\tau_{ksi}^{(j)}}^{k_sT_s+(i-1)T_f+\tau_{ksi}^{(j)}+\delta_{ksi}^{(j)}} \times \exp[A(k_sT_s + T_s - \lambda)]B^{(j)}u_{wi}^{(j)}(\lambda)\,d\lambda$$

$$= G_N^N x_w(k_sT_s) + \sum_{i=1}^{N}\sum_{j=1}^{m}\bar{H}_{wi}^{(j)}\bar{u}_M^{(j)} \tag{41}$$

where

$$\bar{H}_{wi}^{(j)} = G_N^{N-i}\left\{\exp\left[A\left(T_f - \tau_{ksi}^{(j)} - \delta_{ksi}^{(j)}\right)\right]\right\}\left\{\exp\left[A\left(\delta_{ksi}^{(j)}\right)\right] - I_n\right\}A^{-1}B^{(j)}$$

To match the state $x_d(t)$ in Eq. (39) with the state $x_w(t)$ in Eq. (38a), we let the states $x_d(k_sT_s + T_s)$ and $x_d(k_sT_s)$ in Eq. (40) be equal to the states $x_w(k_sT_s + T_s)$ and $x_w(k_sT_s)$ in Eq. (41), respectively. As a result, we have

$$\bar{H}_i^{(j)}\bar{u}_{di}^{(j)}(k_sT_s) = H_{wi}^{(j)}\bar{u}_M^{(j)} \tag{42a}$$

hence,

$$[\exp(AT_f) - I_n]A^{-1}B^{(j)}\bar{u}_{di}^{(j)}(k_sT_s) = \exp\left[A\left(T_f - \tau_{ksi}^{(j)} - \delta_{ksi}^{(j)}\right)\right] \times \left\{\exp\left[A\left(\delta_{ksi}^{(j)}\right)\right] - I_n\right\}A^{-1}B^{(j)}\bar{u}_M^{(j)} \tag{42b}$$

Taking the second-order Taylor-series expansion of the matrix exponential functions in Eq. (42b), we have

$$T_f\left(I_n + \tfrac{1}{2}AT_f\right)u_{di}^{(j)}(k_sT_s) \cong \delta_{ksi}^{(j)}\left[I_n + \tfrac{1}{2}A\left(2T_f - 2\tau_{ksi}^{(j)} - \delta_{ksi}^{(j)}\right)\right]\bar{u}_M^{(j)} \tag{42c}$$

Solving Eq. (42c) yields the desired $\delta_{ksi}^{(j)}$ and $\tau_{ksi}^{(j)}$ in Eq. (38d).

Remark 2: In Ref. 12, a Chebyshev quadrature formula was employed to develop the conventional single-rate state-matching PAM and PWM digital control laws. The conventional digital control laws are computationally simple and able to capture the original system's intersample behavior for a sufficiently small sampling period T_f. The basic requirement of a small sampling interval T_f limits the potential applications of existing PAM and PWM controllers to high-performance systems that require large sampling periods. For example, in the case of low-cost or low-power vehicles requiring a simple computer, the sampling period must be large enough to allow the computations of high-order advanced controllers in real time. This is also the case in controlling high-performance spacecraft, where larger sampling periods are often desirable to limit actuator activity for reducing propellant consumption and to reduce the cost of actuators and sensors. Serious performance degradation is observed when the conventional digital control laws are applied to a system that requires a large sampling period $T_s(=NT_f$ for $N > 1)$.

In this paper, a block-pulse function[20] in Eq. (6) together with an exact integration method in Eq. (29) is utilized to develop lifted multirate state-matching PAM and PWM digital control laws. The developed digital control laws are able to capture the intersample behavior of the original system for a relatively large sampling period $T_s(=NT_f$ for $N > 1)$, although the computational load is heavier than the conventional ones. Note that when the sampling rate $N = 1$, the proposed digital control laws can be reduced to the conventional ones as shown in Eqs. (25), (38c), and (38d) even though the approaches adopted in both digital redesign techniques are different.

III. PAM Controller Redesign of an X-38 LQR

In Ref. 2, an LQR is designed for the subsonic flight test mission of the X-38. This section presents an introduction into the X-38, a brief description of the subsonic mission, and a description of the continuous-time control scheme. The digital redesign of Sec. II is then applied to this continuous-time controller. Although the discrete controller sampling rate being implemented for the X-38 at 25 Hz is fast enough that lifting redesign may not be required, this example is presented to show how the controller could be implemented with a slower sampling rate.

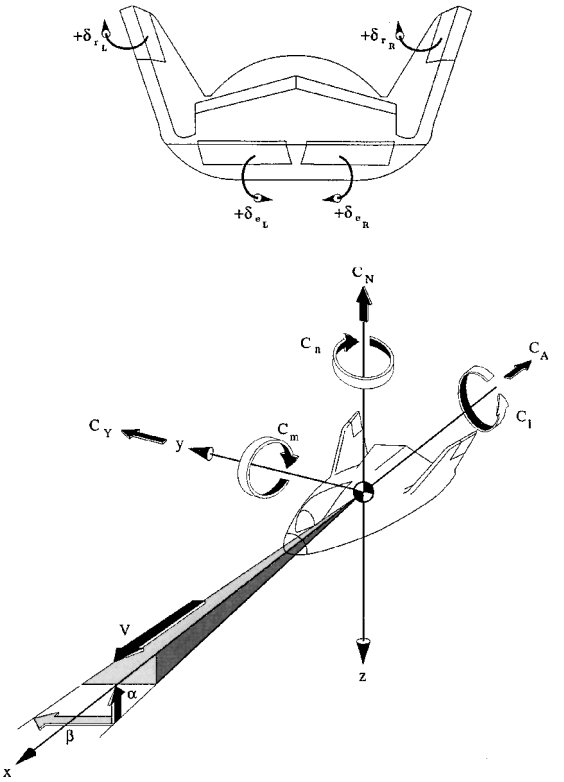

Fig. 3 X-38 control surfaces and body axes coordinate definition.

A. Vehicle Description

The X-38 is the unpowered lifting body vehicle depicted in Fig. 3. It is 23 ft in length and weighs 14,250 lb, having a maximum L/D of roughly 2 at an angle of attack of 12 deg. This craft has a high-quality suite of sensors providing accurate measurements, so that in the design phase, perfect state information is assumed.

The roll and yaw dynamics of this vehicle are highly coupled. The dihedral in the rudder surface causes additional coupling (roll reversal) as they are actuated.[2] Because of these effects, the LQR is applied to the overall system with no separation of the lateral and longitudinal dynamics. The X-38 contains four aerodynamic control surfaces. These four control surfaces, left and right rudder and left and right elevon, are depicted in Fig. 3. Elevator, aileron, and rudder control deflections are defined, respectively, by

$$\delta_e \triangleq \tfrac{1}{2}\left(\delta_{e_L} + \delta_{e_R}\right) \tag{43a}$$

$$\delta_a \triangleq \delta_{e_L} - \delta_{e_R} \tag{43b}$$

$$\delta_r \triangleq \tfrac{1}{2}\left(\delta_{r_L} + \delta_{r_R}\right) \tag{43c}$$

The actuation system for each of the control surfaces is an electromechanical actuator.

The state space describing the vehicle for this mission contains the three rotational velocities (p = roll rate, q = pitch rate, and r = yaw rate), in radians per second, and the three translational velocities (V = velocity in feet per second, α = angle of attack in radians, and β = yaw in radians). Also included are the three attitude positions (ϕ = bank angle, θ = pitch angle, and ψ = heading angle) in radians, and the Earth-relative positions (h = altitude, x = downrange position, and y = crossrange position) in feet. Several vehicle states and (positive) angle rotations are depicted in the lower half of Fig. 3.

B. Mission Description

The subsonic mission for this vehicle is for gliding flight from a B-52 drop at 41,214 ft and Mach 0.67 down to 20,000 ft and Mach 0.57 where the parafoil will deploy for landing. This paper is only concerned with the aerodynamically controlled portion of the flight. The parafoil guidance and control is being designed as a separate system.

Although this vehicle is based on the X-24A, this will be the first set of flights for this exact airframe design. Keeping this in mind, the guidance for this mission is to track a constant angle of attack of 12 deg while flying a coordinated ($\beta = 0$) wings-level trajectory ($\phi = 0$). Downrange and crossrange stay well within landing zone requirements of the dry lake at Edwards Air Force Base.

C. X-38 Model

The X-38 dynamical equations are presented in Ref. 2, but can be written in the form

$$\dot{X} = F(X, U) \tag{44a}$$

$$X(t_0) \equiv X_0 \tag{44b}$$

$$t_0 \equiv \text{given} \tag{44c}$$

The tracking output equation is defined as

$$Y = CX \tag{45}$$

where C is a constant time-invariant matrix of dimension l. The Y output will be used to define the variables to be tracked. In Eqs. (44a) and (44b), $X(t) \in \Re^n$ are the states, $U(\cdot) \in \mathcal{U}$, where $U(t) \in \Re^m$ are the controls (where the class of admissible controls $\mathcal{U}$ is the set of piecewise continuous controls) and t is the time, with t_0 the initial time. The function F is a known function of its arguments and is assumed to be piecewise continuously differentiable. It is further assumed that the optimal control is normal,[24] that there is perfect knowledge of the state variables and system parameters, and that the state initial conditions are known.

The state equation (44a) is linearized by expanding in a singular perturbation about a trim condition (a desired flight condition). Neglecting higher-order terms, the trim equations become

$$\dot{\overset{0}{X}} = F(\overset{0}{X}, \overset{0}{U}) \tag{46a}$$

$$\overset{0}{Y} = C\overset{0}{X} \tag{46b}$$

where the overscript (^{0}) is used to denote the trim condition. The perturbed equations are

$$\dot{x} = F_X(\overset{0}{X}, \overset{0}{U})x + F_U(\overset{0}{X}, \overset{0}{U})u \tag{47a}$$

$$y = Cx \tag{47b}$$

For the trim condition consisting of

$$\begin{aligned}\left[\delta_{e_L}, \delta_{e_R}, \delta_{r_L}, \delta_{r_R}, p, q, r, V, \alpha, \beta, \phi, \theta, \psi, h, x, y\right]^T \\ = [26.89 \text{ deg}, 26.89 \text{ deg}, 0 \text{ deg}, 0 \text{ deg}, 0 \text{ deg/s}, \\ 0 \text{ deg/s}, 0 \text{ deg/s}, 680 \text{ ft/s}, 12 \text{ deg}, 0 \text{ deg}, 0 \text{ deg}, \\ -18.22 \text{ deg}, -43.09 \text{ deg}, 41{,}741 \text{ ft}, 0 \text{ ft}, 0 \text{ ft}]^T\end{aligned} \tag{48}$$

the system matrices A and B are (for angular units in radians)

$$A = \begin{bmatrix} -0.242 & -0.0142 & 0.150 & 0.644E{-}05 & -0.0720 & -26.4 & 0 & 0 & 0 & 0 & 0 \\ -0.00239 & -0.280 & 0.00176 & 0.127E{-}03 & -1.42 & -0.249 & 0 & 0 & 0 & 0 & 0 \\ 0.0358 & 0.00137 & -0.0843 & -0.622E{-}06 & 0.00696 & 1.39 & 0 & 0 & 0 & 0 & 0 \\ 0 & 0 & 0 & -0.375E{-}01 & 3.63 & 0 & 0 & -27.7 & 0 & 0 & 0 \\ 0 & 1 & 0 & -0.947E{-}04 & -0.129 & 0 & 0 & 0.0237 & 0 & 0 & 0 \\ 0.208 & 0 & -0.978 & 0 & 0 & -0.0544 & 0.0448 & 0 & 0 & 0 & 0 \\ 1 & 0 & -0.329 & 0 & 0 & 0 & 0 & 0 & 0 & 0 & 0 \\ 0 & 1 & 0 & 0 & 0 & 0 & 0 & 0 & 0 & 0 & 0 \\ 0 & 0 & 0 & 0 & 1 & 0 & 0 & 0 & 0 & 0 & 0 \\ 0 & 0 & 0 & 0 & 0 & 1 & 0 & 0 & 0 & 0 & 0 \\ 0 & 0 & 0 & 0 & 0 & 0 & 1 & 0 & 0 & 0 & 0 \end{bmatrix} \tag{49a}$$

$$B = \begin{bmatrix} 1.50 & -1.66 & 2.90 \\ -1.64 & -1.66 & 0.0312 \\ 0.00866 & 0.00750 & -1.01 \\ -5.31 & -5.31 & 0 \\ -0.0155 & -0.0155 & 0 \\ 0.000158 & -0.000158 & 0.00550 \\ 0 & 0 & 0 \\ 0 & 0 & 0 \\ 0 & 0 & 0 \\ 0 & 0 & 0 \\ 0 & 0 & 0 \end{bmatrix} \tag{49b}$$

In this design, the state space is augmented by three with the integral of the α, β, and ϕ tracking errors. This technique is used to reduce the steady-state error of the tracking controller.[19] The integral error contains an antiwindup algorithm that limits the windup due to actuator saturation.[3,19] The control vector is

$$\boldsymbol{u}_c = \left[\delta_{e_L}, \delta_{e_R}, \delta_r\right]^T \tag{50}$$

The open-loop poles of this vehicle are

$$\begin{aligned}\lambda(A) = \{&0, 0, 0, -0.1161 \pm 2.6123i, -0.1914 \pm 1.1859i, \\ &-0.0312 \pm 0.0528i, -0.0750 \pm 0.0792i\}\end{aligned} \tag{51}$$

One goal of the control design is to move the poles to the left (for stability) and to increase damping.

D. Linear Tracking Control

Using the trim condition from the preceding section, Eq. (47a) becomes a time invariant linear equation of the form

$$\dot{x}_c = Ax_c + Bu_c \tag{52a}$$

$$y_c = Cx_c \tag{52b}$$

where $x_c = [p, q, r, V, \alpha, \beta, \phi, \theta, \int\alpha, \int\beta, \int\phi]^T$; $u_c = [\delta_{e_L}, \delta_{e_R}, \delta_r]^T$; $y_c = [p, q, r, \alpha, \beta, \phi, \int\alpha, \int\beta, \int\phi]^T$ with $C \in R^{9\times 11}$; and system parameters (A, B) are shown in Eqs. (49a) and (49b). An LQR assuming perfect information is designed in Ref. 2 for the X-38. The tracking problem is to find the optimal control u_c for the system (52a) and (52b) such that the output y_c tracks the commanded signal $\tilde{y}\,[=r(t)$, a reference input in Eq. (3)] minimizing the performance index in Eq. (2). The optimal control law $u_c(t)$ is shown in Eq. (3) with the control gains K_c and E_c shown in Eqs. (4a) and (4b).

E. Controller Design

The control scheme is presented in the block diagram of Fig. 4. The elements with dashed lines represent the portion of the controller

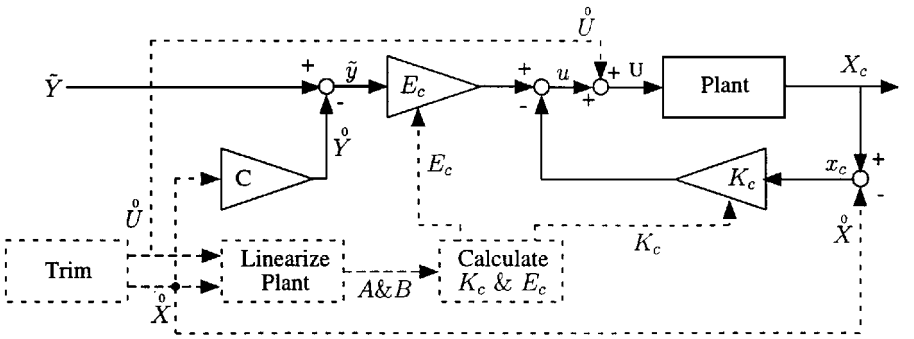

Fig. 4 Control system block diagram.

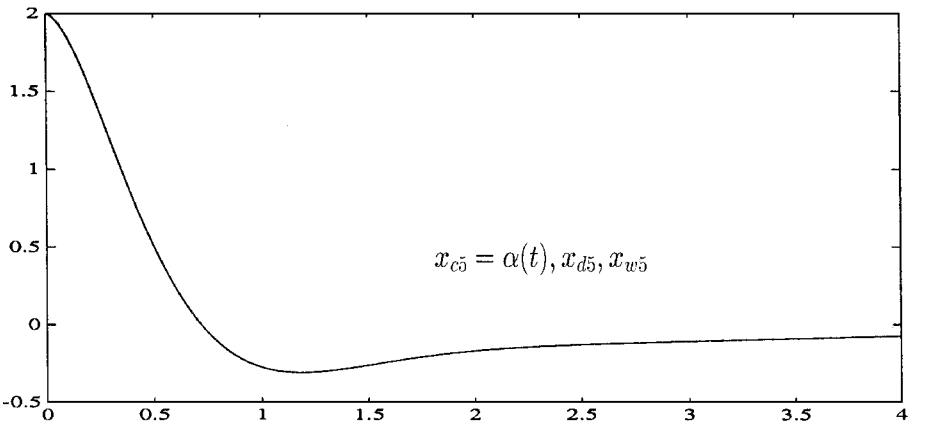

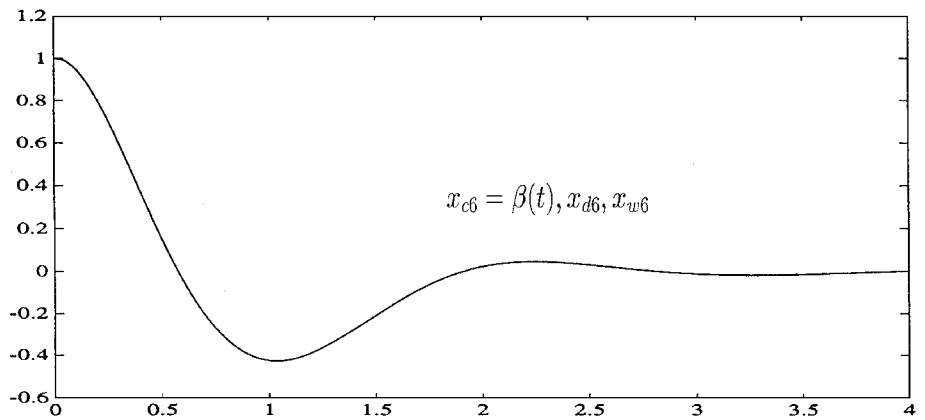

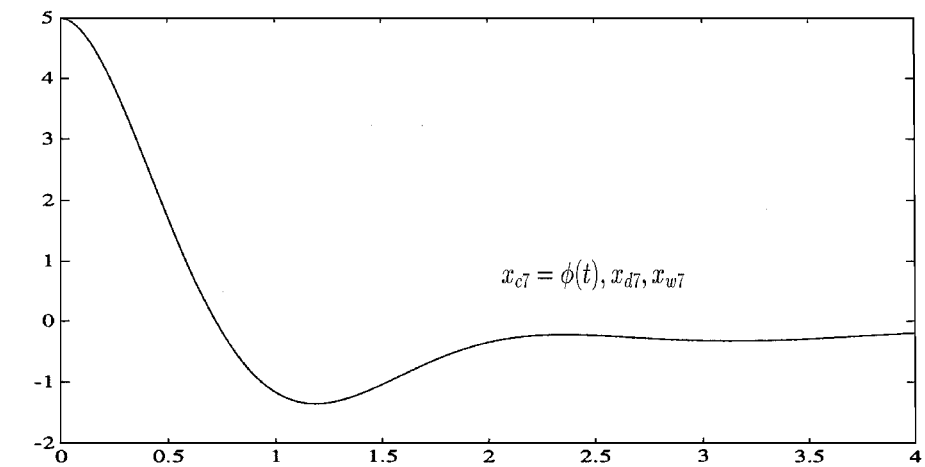

Fig. 5 Linear simulation tracking histories.

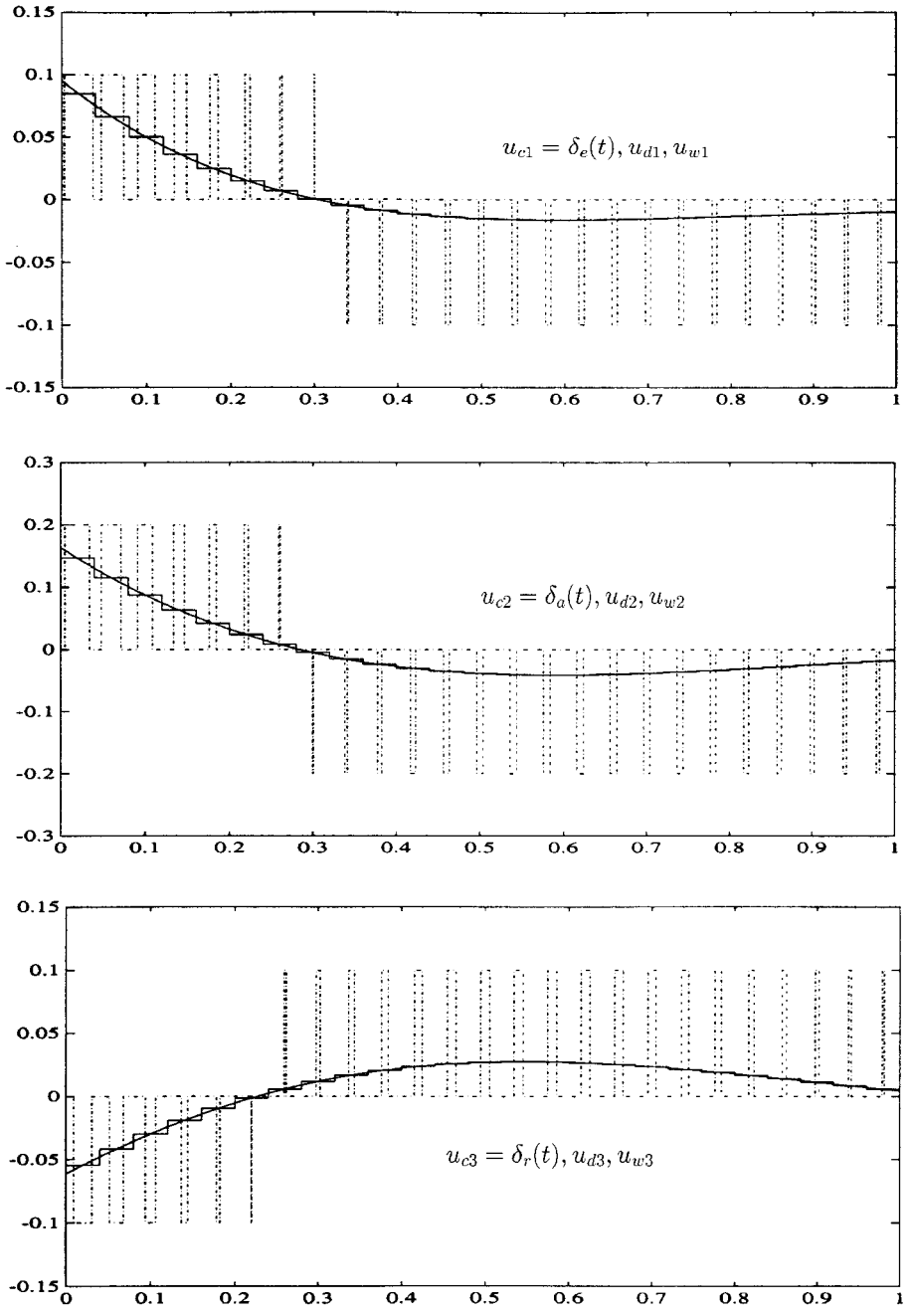

Fig. 6 Linear simulation control histories.

that is processed off-line, That is, trim and linearization are performed prior to turning on the controller.

The control weights Q and R in Eq. (2) were chosen through a trial and error method. The rudder, elevator, and aileron on this vehicle are nearly equally effective; therefore, their weights (in R) are chosen as 1. The variables chosen to be tracked are α, β, and ϕ. The tracking error weights Q were chosen by limiting the rate of change of tracking (by weights on the body rates), weights on the tracking variables themselves, and weights on the integrals of the tracking errors. The expected response would be a bit like proportional-integral-derivative control. Because mission design dictates level coordinated flight, cross coupling weights were chosen for the proportional and integral error of α. Adjusting these cross coupling weights provided gains in E_c giving the desired tracking. Similar cross coupling could be added for β and ϕ if it was desired for them to track something other than a zero command. The weighting matrices are $R = I_{3\times 3}$ and

$$C^T QC = \begin{bmatrix} 0.0700 & 0 & 0 & 0 & 0 & 0 & 0 & 0 & 0 & 0 & 0 \\ 0 & 0.7 & 0 & 0 & 0 & 0 & 0 & 0 & 0 & 0 & 0 \\ 0 & 0 & 7 & 0 & 0 & 0 & 0 & 0 & 0 & 0 & 0 \\ 0 & 0 & 0 & 0 & 0 & 0 & 0 & 0 & 0 & 0 & 0 \\ 0 & 0 & 0 & 0 & 28 & 0 & 0 & 0 & 10.5 & 0 & 0 \\ 0 & 0 & 0 & 0 & 0 & 0.007 & 0 & 0 & 0 & 0 & 0 \\ 0 & 0 & 0 & 0 & 0 & 0 & 2.1 & 0 & 0 & 0 & 0 \\ 0 & 0 & 0 & 0 & 0 & 0 & 0 & 0 & 0 & 0 & 0 \\ 0 & 0 & 0 & 0 & 10.5 & 0 & 0 & 0 & 4.2 & 0 & 0 \\ 0 & 0 & 0 & 0 & 0 & 0 & 0 & 0 & 0 & 0.7 & 0 \\ 0 & 0 & 0 & 0 & 0 & 0 & 0 & 0 & 0 & 0 & 0.7 \end{bmatrix} \tag{53}$$

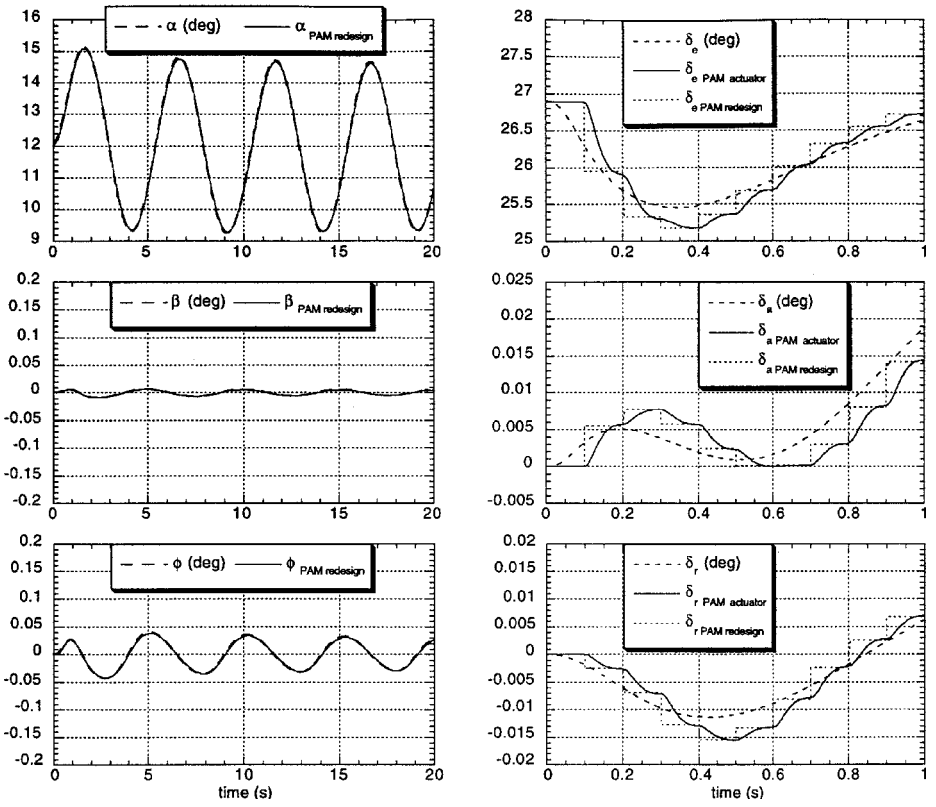

Fig. 7 Tracking comparison of continuous and redesigned controllers.

The Riccati equation (5) arising in the LQR problem is solved using a Schur decomposition.[19] These choices of Q and R give the following gains:

$$K_c = \begin{bmatrix} 0.463 & -1.51 & 1.55 & 0.0001 & -3.72 & -4.41 & 1.28 & -0.0382 & -1.45 & 0.228 & 0.548 \\ -0.450 & -1.49 & -1.55 & 0.0001 & -3.74 & 4.41 & -1.26 & -0.0377 & -1.45 & -0.228 & -0.544 \\ -0.172 & -0.00132 & -5.47 & 0.0000001 & -0.00737 & 8.18 & -0.933 & -0.00002 & -0.00247 & 0.772 & -0.322 \end{bmatrix} \tag{54a}$$

$$E_c = \begin{bmatrix} 0 & 0 & 0 & -3.61 & 0 & 0 & -1.45 & 0.228 & 0.548 \\ 0 & 0 & 0 & -3.63 & 0 & 0 & -1.45 & -0.228 & -0.544 \\ 0 & 0 & 0 & -0.00616 & 0 & 0 & -0.00247 & 0.772 & -0.322 \end{bmatrix} \tag{54b}$$

for a tracking vector of $(p, q, r, \alpha, \beta, \phi, \int\alpha, \int\beta, \int\phi)^T$. The resulting closed-loop eigenvalues are

$$\lambda(A - BK_c) = \{-1.3530 \pm 2.8313i, -2.5317 \pm 2.4605i, -2.1184, -1.3872, -0.6001, -0.3850, -0.0828, -0.0307 \pm 0.0510i\} \tag{55}$$

Comparing Eqs. (55) and (51), it can be seen that indeed the poles have been moved to the left.

F. Redesign

It is desirable to find the lifted dual-rate PAM and PWM digital controllers for the linearized model in Eqs. (52a) and (52b) with the parameters in Eqs. (49a) and (49b). For the linear simulation, the system transient response is investigated. Redesigned PAM and PWM controllers are applied to the linear system with the perturbed initial condition $x_c(0) = [0, 0, 0, 0, 2 \text{ deg}, 1 \text{ deg}, 5 \text{ deg}, 0, 0, 0, 0]^T$ with $T_f = 0.04$ s and $T_s = NT_f = 0.16$ s for $N = 4$. The output of the digitally controlled linearized system tracks the linearized commanded signal $r(t) = 0$. In addition, it is desirable to carry out digital simulations of the digitally controlled original nonlinear dynamic model of X-38 shown in Eqs. (44a), (44b), and (45) using the aforementioned PAM digital controller.

IV. Results

The digitally redesigned PAM control gains K_{dk} in Eq. (24d) and E_{dk} in Eq. (24e) for $T_f = 0.04$ s are

$$K_{dk} = \begin{bmatrix} 0.4541 & -1.4271 & 1.5491 & 0.0001 & -3.3352 & -4.4163 & 1.2441 & -0.0362 & -1.3091 & 0.2263 & 0.5304 \\ -0.4419 & -1.4049 & -1.5544 & 0.0001 & -3.3525 & 4.5306 & -1.2264 & -0.0357 & -1.3084 & -0.2255 & -0.5269 \\ -0.1397 & -0.0028 & -5.0586 & 0.0000 & -0.0109 & 7.2852 & -0.8295 & -0.0001 & -0.0037 & 0.6993 & -0.2855 \end{bmatrix} \tag{56a}$$

$$E_{dk} = \begin{bmatrix} 0 & 0 & 0 & -3.2586 & 0 & 0 & -1.3091 & 0.2263 & 0.5304 \\ 0 & 0 & 0 & -3.2763 & 0 & 0 & -1.3084 & -0.2255 & -0.5269 \\ 0 & 0 & 0 & -0.0092 & 0 & 0 & -0.0037 & 0.6993 & -0.2855 \end{bmatrix} \tag{56b}$$

Also, the desired lifted gains $\bar{K}_d^{(N)}$ in Eq. (24b) and $\bar{E}_d^{(N)}$ in Eq. (24c) with $N=4$ and $T_s=0.16$ s for the lifted dual-rate PAM digital control law in Eq. (24) can be computed using K_{dk} and E_{dk} in Eqs. (56a) and (56b) and $\hat{G}_{cN}$ and $\hat{H}_{cN}$ in Eq. (24).

Figure 5 shows the comparisons of the states using the continuous controller, $x_{c5}(t)$ [$\alpha(t)$, the angle of attack] in Eq. (52) and the corresponding digitally controlled states $x_{d5}(t)$ in Eq. (22) and $x_{w5}(t)$ in Eq. (38a) via the respective analog control law in Eq. (3), the lifted dual-rate PAM digital controller in Eq. (24), and PWM digital controller in Eq. (38c) having $T_f=0.04$ s, $N=4$, $T_s=NT_f=0.16$ s, $\bar{u}_M^{(1)}=0.1$, $\bar{u}_M^{(2)}=0.2$, and $\bar{u}_M^{(3)}=0.1$ for the linearized model in Eq. (52). It is easily seen that the three state histories lie right on top of each other. The comparisons of the associated analog control signal $u_c(t)$ in Eq. (3) with the digital signal in Eq. (4), $\bar{\boldsymbol{u}}_d^{(N)}(k_sT_s)$ in Eq. (24) and $u_{wi}^{(j)}(\lambda)$ in Eq. (38c) are shown in Fig. 6 with an expansion of the timescale for ease of viewing.

The nonlinear simulation results are shown in Fig. 7. For an α tracking command of 12 deg + 3 deg sin($2\pi t/5$) [all other elements of $r(t)=0$], it can be seen that the lifted dual-rate PAM control law tracking histories of $\alpha(t)$, $\beta(t)$, and $\phi(t)$ sit right on top of the continuous-time tracks. The control surface histories for the two controllers are also shown in Fig. 7, where the dashed line depicts the continuous-time control surfaces. The dotted line depicts the lifted dual-rate PAM actuator commands, and the solid line shows the actuator output for the lifted dual-rate PAM control. For physical insight, the control surfaces defined by Eq. (43) are depicted in Fig. 7 instead of the elements of the control vector (50). Once again, the time scale for the control history has been expanded for clarity. The coupled dynamics of this vehicle can be seen in Fig. 7 as both β and ϕ undergo slight oscillation at the α excitation frequency. The magnitude of this oscillation is acceptable for this vehicle and mission.

Additional digital simulations of the original nonlinear dynamic model of X-38 using various PAM digital controllers have been carried out. It was observed that when $T_s=NT_f=T_f=0.4$ s for $N=1$, the single-rate PAM controller for the linearized model in Eq. (52) gives a good tracking trajectory, whereas for the original nonlinear dynamic model of X-38 in Eqs. (44) and (45), it was unstable. However, when $T_s=NT_f=0.4$ s and $T_f=0.1$ s for $N=4$, the lifted dual-rate PAM controller provides good tracking trajectories for both the linearized model in Eq. (52) and the original nonlinear dynamic model of X-38 in Eqs. (44) and (45). Nevertheless, for too large a sample time, for example $T_s=1.6$ s and $N=4$, the nonlinear model of the X-38 in Eqs. (44) and (45) is closed-loop unstable.

V. Conclusions

A new state-matching digital redesign method has been developed to find the lifted dual-rate PAM and PWM digital controllers[5] from the continuous-time optimal controllers for the X-38 (the NASA prototype re-entry vehicle). The proposed digital controllers are able to closely match the intersample states of the continuous-time controlled analog system with those of the digitally controlled sampled-data system. The proposed method provides us an alternative methodology to perform indirect digital design of state-feedback multivariable continuous-time systems and enables us to implement the analog controllers using digital controllers. The nonlinear dynamical model of the X-38 has been utilized as a test bed for digital simulations of the newly developed digital controllers. The digitally controlled X-38 is able to robustly track the desired trajectory while remaining insensitive to parameters, initial conditions, and exogenous disturbances.

Acknowledgment

This work was supported by the U.S. Army Research Office, Grant DAAG-55-98-1-0198. The authors wish to express their gratitude for valuable remarks and suggestions made by reviewers and L. G. Bushnell, Mathematical and Computer Sciences Division, U.S. Army Research Office.

References

[1]Wilson, J. R., "CRV Investment Offers Safe Return," *Aerospace America*, No. 6, 1997, pp. 28–32.

[2]Bain, J., and Sunkel, J., "Autonomous Control for Subsonic Flight of the X-38," AIAA Paper 98-4567, Aug. 1998.

[3]Astrom, K. J., and Wittenmark, B., *Computer Controlled Systems*, Prentice–Hall, Englewood Cliffs, NJ, 1997, pp. 293–368.

[4]Houpis, C. H., and Lamont, G. B., *Digital Control Systems*, McGraw–Hill, New York, 1985, pp. 235–249.

[5]Kuo, B. C., *Digital Control Systems*, Holt, Rinehart, and Winston, New York, 1980, pp.321–338, 404, 405.

[6]Skaar, S. B., Tang, L., and Yalda-Mooshabad, I., "On–Off Attitude Control of Flexible Satellites," *Journal of Guidance, Control, and Dynamics*, Vol. 9, No. 4, 1986, pp. 507–510.

[7]Anthony, T. C., Wie, B., and Carroll, S., "Pulse Modulated Control Synthesis for a Flexible Structure," *Proceedings of the AIAA Guidance, Navigation, and Control Conference*, AIAA, Washington, DC, 1989, pp. 65–76.

[8]Bamieh, B., Pearson, B. J., Francis, B., and Tannenbaum, A., "A Lifting Technique for Linear Periodic Systems with Applications to Sampled-Data Control," *Systems and Control Letters*, Vol. 17, No. 1, 1991, pp. 79–88.

[9]Bernelli-Zazzera, F., and Mantegazza, P., "Pulse Width Equivalent to Pulse Amplitude Discrete Control of Linear Systems," *Journal of Guidance, Control, and Dynamics*, Vol. 15, No. 2, 1992, pp. 461–467.

[10]Bernelli-Zazzera, F., Mantegazza, P., and Nurzia, V., "Multi-Pulse-Width Modulated Control of Linear Systems," *Journal of Guidance, Control, and Dynamics*, Vol. 21, No. 1, 1998, pp. 64–70.

[11]Sunkel, J. W., Shieh, L. S., and Zhang, J. L., "Digital Redesign of an Optimal Momentum Management Controller for the Space Station," *Journal of Guidance, Control, and Dynamics*, Vol. 14, No. 4, 1991, pp. 712–723.

[12]Shieh, L. S., Wang, W. M., and Sunkel, J. W., "Design of PAM and PWM Controllers for Sampled-Data Interval Systems," *Journal of Dynamic Systems, Measurement and Control*, Vol. 118, No. 4, 1996, pp. 673–682.

[13]Fujimoto, H., Kawamura, A., and Tomizuka, M., "Proposal of Generalized Digital Redesign Method in Use of N-Delay Control," *Proceedings of the American Control Conference*, IEEE Control Systems Society, Piscataway, NJ, 1997, pp. 3200–3204.

[14]Rafee, N., Chen, T., and Malik, O. P., "A Technique for Optimal Digital Redesign of Analog Controllers," *IEEE Control Systems Technology*, Vol. 5, No. 1, 1997, pp. 89–99.

[15]Chen, T., and Francis, B. A., *Optimal Sampled-Data Control Systems*, Springer–Verlag, New York, 1995, pp. 171–245.

[16]Delfeld, F. R., and Murphy, G. J., "Analysis of Pulse-Width-Modulated Control Systems," *Institute of Radio Engineers Trans.*, Vol. AC-6, No. 3, 1961, pp. 283–292.

[17]Anderson, B. D. O., "Controller Design: Moving from Theory to Practice," *IEEE Control Systems Magazine*, Vol. 13, No. 4, 1993, pp. 16–25.

[18]Moore, K. L., Bhattacharyya, S. P., and Dahleh, M., "Capabilities and Limitations of Multirate Control Schemes," *Automatica*, Vol. 29, No. 4, 1993, pp. 941–951.

[19]Lewis, F. L., *Optimal Control*, Wiley, New York, 1986, pp. 222–224.

[20]Shieh, L. S., Yeung, C. K., and McInnis, B. C., "Solution of State-Space Equations Via Block-Pulse Functions," *International Journal of Control*, Vol. 28, No. 3, 1978, pp. 383–392.

[21]Polites, M. E., "Ideal State Reconstructor for Deterministic Digital Control Systems," *International Journal of Control*, Vol. 49, No. 6, 1989, pp. 2001–2011.

[22]Shieh, L. S., Chen, G. C., and Tsai, J. S. H., "Hybrid Suboptimal Control of Multi-Rate Multi-Loop Sampled-Data Systems," *International Journal of Systems Science*, Vol. 23, No. 6, 1992, pp. 839–854.

[23]Mita, T., "Optimal Digital Feedback Control System Counting Computation Time of Control Laws," *IEEE Transactions on Automatic Control*, Vol. AC-30, No. 6, 1985, pp. 542–548.

[24]Bryson, A. E., and Ho, Y. C., *Applied Optimal Control*, Hemisphere, Washington, DC, 1975, pp. 181, 182.